Heliyon 9 (2023) e16436

Contents lists available at ScienceDirect

Heliyon

journal homepage: www.cell.com/heliyon

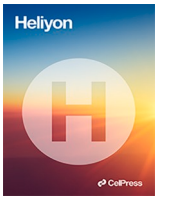

Research article

Cellulose nanocrystals from agricultural residues (*Eichhornia crassipes)*: Extraction and characterization

Mohamed H. Hemida [a,*], Hesham Moustafa [b,c], Sherif Mehanny [d], Mohamed Morsy [e,f], Alain Dufresne [g], Eid N. Abd EL Rahman [a], M.M. Ibrahim [a]

[a] *Agricultural Engineering Department, Faculty of Agriculture, Cairo University, Egypt*
[b] *Department of Polymer Metrology & Technology, National Institute of Standards (NIS), Tersa Street, El Haram, P.O Box 136, Giza, 12211, Giza, Egypt*
[c] *Bioanalysis Laboratory, National Institute of Standards (NIS), Tersa Street, El Haram, P.O Box 136, Giza, 12211, Giza, Egypt*
[d] *Department of Mechanical Design and Production, Faculty of Engineering, Cairo University, Egypt*
[e] *Building Physics and Environment Institute, Housing and Building National Research Center (HBRC), Dokki, Giza, Egypt*
[f] *Nanotechnology Research Center (NTRC), The British University in Egypt (BUE), El Sherouk City, Suez Desert Road, Cairo, 11837, Egypt*
[g] *Université Grenoble Alpes, CNRS, Grenoble INP, LGP2, F-38000, Grenoble, France*

A R T I C L E I N F O

Keywords:
Cellulose nanocrystals extraction
Agricultural residues
XPS analysis
Transmission electron microscopy
Acid hydrolysis
Nile rose

A B S T R A C T

Extraction of cellulose nanocrystals (CNCs) from agro-residues has received much attention, not only for their unique properties supporting a wide range of potential applications, but also their limited risk to global climate change. This research was conducted to assess Nile roses (*Eichhornia crassipes*) fibers as a natural biomass to extract CNCs through an acid hydrolysis approach. Nile roses fibers (NRFs) were initially subjected to alkaline (pulping) and bleaching pretreatments. Microcrystalline cellulose (MCC) was used as control in comparison to Nile rose based samples. All samples underwent acid hydrolysis process at a mild temperature (45 °C). The impact of extraction durations ranging from 5 to 30 min on the morphology structure and crystallinity index of the prepared CNCs was investigated. The prepared CNCs were subjected to various characterization techniques, namely: X-ray diffraction (XRD), FT-IR analysis, Transmission electron microscopy (TEM), and X-ray Photoelectron spectroscopy (XPS). The outcomes obtained by XRD showed that the crystallinity index increased as the duration of acid hydrolysis was prolonged up to 10 min, and then decreased, indicating optimal conditions for the dissolution of amorphous zones of cellulose before eroding the crystallized domains. These data were confirmed by FT-IR spectroscopy. However, a minor effect of hydrolysis duration on the degree of crystallinity was noticed for MCC based samples. TEM images illustrated that a spherical morphology of CNCs was formed as a result of 30 min acid hydrolysis, highlighting the optimal 20 min acid hydrolysis to obtain a fibrillar structure. The XPS study demonstrated that the main constituents of extracted CNCs were carbon and oxygen.

1. Introduction

Due to global warming effects, raising greater environmental attention, biomass and agro-residues became the most valuable

* Corresponding author.
E-mail address: mohamed.h.hemida@agr.cu.edu.eg (M.H. Hemida).

https://doi.org/10.1016/j.heliyon.2023.e16436
Received 27 October 2022; Received in revised form 11 May 2023; Accepted 16 May 2023
Available online 25 May 2023

alternative to address substantial health threat to humanity because of increasing greenhouse gases (GHG) emissions, such as carbon dioxide, methane and nitrous oxide [1]. These GHG are one of the main contributors to climate change, which according to World Health Organization (WHO) in 2021 could cause about 250,000 additional deaths per year due to heat stress between 2030 and 2050. In addition, the accumulation of agro-residues poses disposal problems in landfill zones and causes serious environmental issues if burned in open air. Nevertheless, agro-residues are considered as lignocellulosic biomass and consist mainly of cellulose, hemicelluloses, lignin, besides other organic matters [2,3]. Currently, considerable works [4–6][7] have been conducted on agro-residues for reducing the risks associated with their disposal, and to promote their use in biofuels, construction, polysaccharide productions, and animal feed. Also, it was found that pyrolysis of these biomasses can yield biochar, bio-oil and bio-diesel [8]. Nowadays, they are used as additive or reinforcing material in biopolymers [9–11][12,13]. The aforementioned applications stem from their sustainable, biodegradable, harmless and low-cost nature [14]. Moreover, they contain a large amount of ash compared to other types of biomass such as poultry waste and algae [15]. All these features have allowed the use of these biomasses in promising applications such as renewable energy production [16], food-packaging [17], bio-membranes for protein purification, and other biomedical purposes [18].

Cellulose, considered as a natural polymer, is found in the cell wall of plants and plays a pivotal role in increasing the strength and rigidity of the cell wall [19,20]. Several processes [21–23] have been conducted on cellulose not only for extracting cellulose nanocrystals (CNCs), but also to convert it into valuable materials. CNCs are extracted from numerous renewable resources including plants, but also some animals and algae [24]. Among these resources, Nile Roses or *Eichhornia crassipes,* which grow on the surface of river water, are used as a natural resource to extract CNCs in this work. These plants have green leaves, rapid growth and high reproduction in the freshwater environment. This makes them one of the most invasive and widespread aquatic weeds. In Egypt, Nile roses plants caused aquatic disasters in the Nile river because of their high water consumption (i.e. ~ 3.5 billion cubic meters per year in Egypt) [25]. Furthermore, the growth rate of these plants can reach about 220 kg/ha/day under normal climatic conditions [26]. For these reasons, we attempt in the present work to produce CNCs as value-added materials from Nile roses plants to reduce their hazardous impact on living organisms in case of water-related disasters.

Numerous methods for extracting CNCs from agro-residues have been reported such as ultrasonic approach, enzymatic hydrolysis, and acid chemical hydrolysis. The latter is the most well-known and most used because it is easy and rapid for producing CNCs with high degree of crystallinity, compared to other techniques [27,28]. However, the CNCs obtained by this method have a small crystal size [29]. The acid hydrolysis process can break the disordered and amorphous parts of cellulose, releasing single crystals. CNCs are mostly needle-shaped particles with at least one dimension typically equal or less than 10 nm. CNCs are highly crystalline in nature compared to cellulose itself and may be referred to as cellulose nano-whiskers, nanocrystalline cellulose or cellulose nanocrystals [27,30]. In some cases, a spherical structure of cellulose nanocrystals can be produced [29]. As CNCs are derived from renewable natural resources, much attention is being paid to their potential applications because they are abundant, low density, biocompatible, non-toxic, biodegradable, and the raw material is low-cost [31]. Furthermore, CNCs possess unique properties such as high strength and stiffness, and barrier behavior. It is noticed from previous literature regarding the acid hydrolysis extraction process that some parameters such as reaction duration, acid concentration, the nature of the acid and temperature can affect the morphological structure and properties of CNCs [27,32].

The Current study aims to extract and characterize CNCs obtained from pre-pulped (alkaline treatment) and pre-bleached Nile Roses fibers (NRFs) by acid hydrolysis with reaction durations ranging from 5 to 30 min at a fixed temperature (i.e. 45°). The impact of acid hydrolysis durations on the crystallinity and morphology of fabricated CNCs was investigated by techniques such as XRD, TEM and XPS analysis. Additionally, the functional properties of native, pulped and bleached fibers were characterized by FTIR spectroscopy. Similar experiments were also performed with pure microcrystalline cellulose (MCC) for comparison.

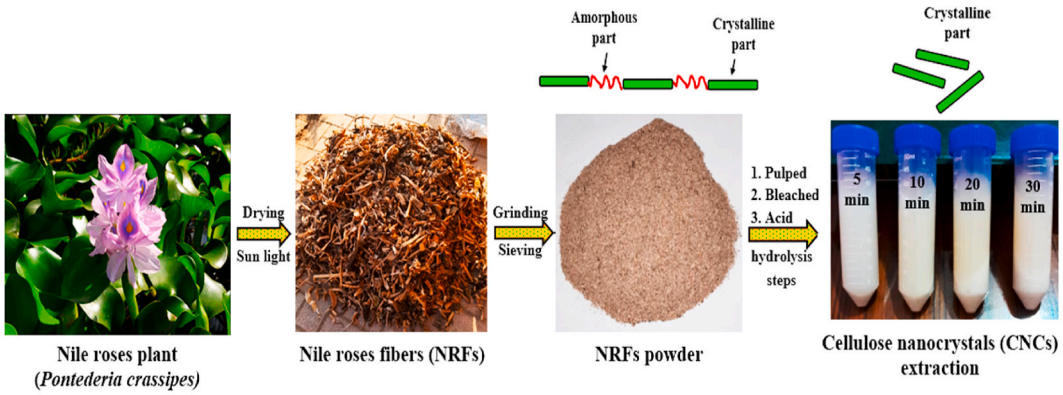

Fig. 1. Extraction processes of cellulose nanocrystals (CNCs) from Nile roses fibers (NRFs).

2. Materials and experimental techniques

2.1. Materials

Nile roses plants were collected from the branches of the Nile water canals in Beni Suef Governorate, Egypt and dried through solar dehydration process until reaching constant weight. The dehydration period lasted one month on house roof, followed by further drying in an oven at 105 °C for 24 h. Sodium hydroxide with a dosage of 98.6% was obtained from Fisher Scientific. It was used for the pulping treatment of the fibers. Acetic acid with 98% purity and sodium chlorite ($NaCLO_2$, 98.8%), used for the bleaching process after fiber pulping treatment, were obtained from Sigma-Aldrich, Egypt. Microcrystalline cellulose (MCC, USP) with density of 1.5 g/cm^3 was purchased from Avi-Chem Industries, Maharashtra, India and used for comparison with CNCs extracted from NRFs.

2.2. Extraction process of cellulose nanocrystals from NRFs

After complete drying, the Nile rose leaves were cut into small pieces and then ground using a laboratory mill (see Fig. 1). The pulping process was performed by mixing 100 g of native fiber with 1.750 L of deionized water (DIW) and 20 g of NaOH. The mixture was heated up to 110 °C for 2 h, and then the fibers were washed thoroughly and dried in an electric oven to a constant weight. The pulped fibers were subjected to a bleaching treatment, performed by mixing 10 g of pulped fiber with 400 mL of DIW with 1.5 g of $NaCLO_2$ (sodium chlorite) and 15 mL of acetic acid. Then, they were put in a water bath for 2 h at 100 °C. The bleaching process was repeated 10 times to obtain perfect white fibers. Both bleached NRFs residues and lab microcrystalline cellulose (MCC) were subjected to acid hydrolysis by adding 3 g of (bleached NRFs or MCC) to 60 mL of 60% w/v) H_2SO_4 (and heated to 45 °C for 5, 10, 20, and 30 min under mechanical stirring. The acid hydrolysis reaction was interrupted by quenching in 1200 mL of ice. Subsequently, the resulting suspension was centrifuged at 4500 rpm for 30 min, simultaneously adding 5% (w/v) $NaHCO_3$ until the pH of the suspension reached 7–8. After that, the supernatant was decanted and replaced with DIW. A 50 mL tube was shaken and recentrifuged. The last two steps were repeated 1–2 times and then the concentrate was stored in glass vials in a laboratory fridge until further investigation was performed. In order to complete this process, many attempts were made in the preliminary phase; nevertheless, generally in documented experiments, three experimental repetitions were conducted for all specimens.

2.3. X-ray diffraction analysis

The CNCs extracted from NRFs and MCC with different acid hydrolysis durations were characterized using PANalytical Empyrean X-ray diffractometer equipped with CuK radiation (30 kV and 10 mA), Netherlands. The diffraction angle varied from $2\theta = 4^\circ$ to 90° with a step size of 0.33°/s. The crystallinity index (CI) was calculated by formula reported elsewhere [33,34], $CI = (I_{cryst}.-I_{am})/I_{cryst}$, where I_{cryst}. is the intensity at the maximum of the diffractogram, corresponding to the (2 0 0) peak and I_{am} is the intensity of the amorphous valley between (2 0 0) and (1 1 0), around $2\theta = 18^\circ$.

2.4. FT-IR spectroscopy

Transmission mode FT-IR spectra were performed to detect the functional groups of the native fiber and its precursors after treatment by acid hydrolysis using a Thermo Scientific Nicolet 380, USA FT-IR spectrometer in the spectral range from 4000 to 400 cm^{-1} with a resolution of 4 cm^{-1} and 32 scans per sample. Samples were prepared by pressing 100 mg of dried KBr and 2–3 mg of powder to obtain a thin disk. Pure KBr disk was used as a reference.

2.5. TEM observations

The morphology and the dimensions of CNCs extracted from NRFs and sourced MCC were investigated using a transmission electron microscopy (JEOL, Model Jem-1400, Japan) with an accelerating voltage of 200 kV. Part of each sample was firstly dispersed in DIW and then a diluted droplet was deposited on the surface of a copper observation grid coated with an amorphous carbon film.

2.6. Zeta potential analysis

The investigated CNCs samples were measured using a Zetasizer Ver.7.02, Malvern, UK. All samples were prepared as follows: 0.5 ml CNC sample solution was taken and diluted 100 times using deionized water, followed by dispersed with ultrasonic treatment for 30 min, and dropped into the sample pool. The average was recorded for three measurements.

2.7. X-ray photoelectron spectroscope (XPS)

XPS analysis was used to determine the surface elemental composition of the prepared samples. XPS spectra were collected with K-Alpha (Thermo Fisher Scientific, USA) with monochromatic X-ray Al K-alpha radiation from 10 to 1350 eV, spot size of 400 μm at pressure of 9–10 mbar with full spectrum pass energy of 200 eV and narrow spectrum 50 eV. Measurements were performed for hydrolysis times of 5 min and 30 min, for both cellulose sources. Study scans were conducted from 1350 to 0 eV, while high-resolution spectra of the O 1s region (525–545) and C 1s region (279–298) were collected with a scan step of 0.1eV.

3. Results and discussion

3.1. X-ray diffraction

The XRD patterns of the different samples were shown in Fig. 2(a and b). For pulped NRFs (Fig. 2(a)), weak peaks are identified around 2θ = 15° and 22°. After the bleaching process, these peaks were broader and more defined, indicating the removal of non-cellulosic materials. Bleached samples that were hydrolyzed for different times exhibited the same peaks and a new peak that appears around 2θ = 35°. These peaks were characteristic of cellulose I (native cellulose) and correspond to (101), (200), and (040) diffraction planes, respectively [35,36]. No alteration of the crystalline structure of cellulose was associated with the bleaching and acid hydrolysis treatments. The structure-related parameters represented in micro-strain (ε), dislocation density (δ), and crystallinity index (X_c) were estimated using equations (1)–(3), respectively [35,37]:

$$\varepsilon = \beta \cos\theta \setminus 4 \tag{1}$$

$$\delta = {}^{1}/_{D^2} \tag{2}$$

$$X_c = \left[\frac{I_{200} - I_{am}}{I_{200}}\right] X\ 100 \tag{3}$$

Where β is the full width at half maximum (FWHM) in radians, D is the average crystallite size in nm, I_{200} represents the maximum intensity of the (200) peak, and I_{am} is the intensity of the amorphous domains determined around 2θ = 18°. Table 1 showed the parameters estimated using the above-mentioned equations. It was observed that the micro-strain and dislocation density both decreased as the duration of the acid hydrolysis treatment increased. The degree of crystallinity (X_C) was calculated to describe the amount of crystalline materials in cellulose extraction from NRFs (Fig. 2(a)) and MCC (Fig. 2(b)). It was used to interpret changes in cellulose structure after physicochemical and biological treatments. It was also found that the crystallinity index increases as the acid hydrolysis time increases to 10 min, and then started to decrease. An optimal value of crystallinity was therefore associated to a 10 min-acid hydrolysis treatment of NRFs (Fig. 3). On the contrary, for MCC samples, the acid hydrolysis time had a minor effect on the crystallinity, as illustrated in Fig. 3. The highest degree of crystallinity was achieved for 10 min bleached sample. Moreover, Table 2 summarized the degree of crystallinity results of extracted CNCs-NRFs and other natural lignocellulosic fibers explained in previous literature. The outcomes of this work exhibited a better crystallinity degree achieved when compared to other literature regardless the treatment method.

3.2. FT-IR analysis

The functional properties of native, pulped and bleached fibers, as well as bleached fibers subjected to acid hydrolysis for different durations can be supported using FT-IR spectroscopy in transmission mode within the 4000 to 400 cm^{-1} wavenumber range, as displayed in Fig. 4(a–c). As depicted in Fig. 4(a), the highlighted absorption peaks for native fiber appearing at ~ 3436 cm^{-1}, 2920 cm^{-1}, 1638 cm^{-1}, 1057 cm^{-1}, and ~727 cm^{-1}, were assigned to –OH stretching, $–CH_2$ symmetric, –OH bending, C–*O*–C vibration in pyranose ring, and aromatic ring in lignin, respectively [11,29,47,48]. After bleaching the native fibers, the intensity of absorption

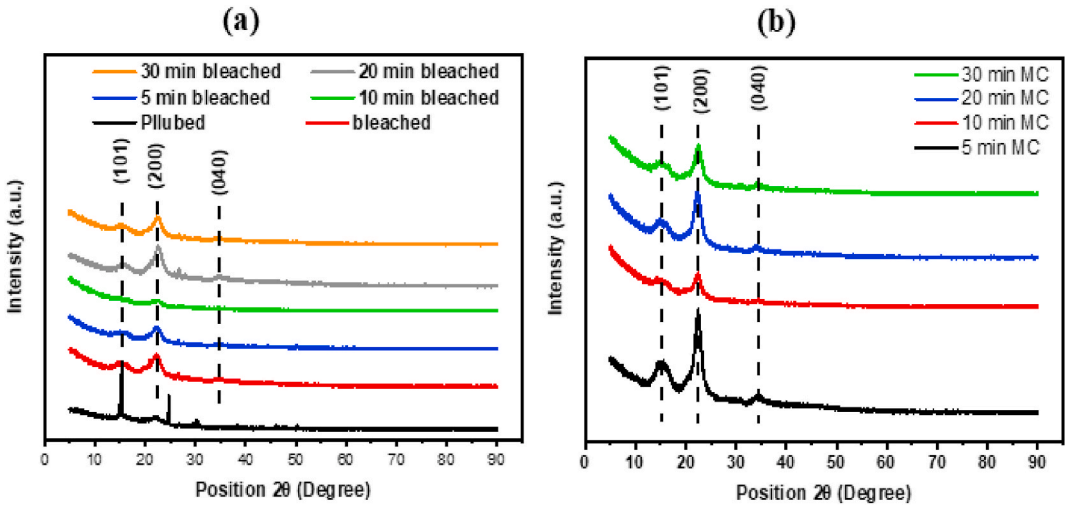

Fig. 2. XRD patterns for (a) pulped, bleached and acid hydrolyzed NRFs with different acid hydrolysis times and (b) MCC samples hydrolyzed for different durations.

Table 1
Structural parameters for CNCs-NRFs and CNCs-MCC samples.

Sample name	(*hkl*)	d-spacing(Å)	ε	δ (nm^{-2})	X_c, %
5 min CNCs-NRFs	(200)	4.05	0.040977	0.051776	65.5
10 min CNCs-NRFs	(200)	3.09	0.039222	0.047437	87.6
20 min CNCs-NRFs	(200)	3.34	0.03857	0.047408	77.1
30 min CNCs-NRFs	(200)	3.35	0.037657	0.044387	67.2
5 min CNCs-MCC	(200)	3.95	0.030381	0.030941	70.6
10 min CNCs-MCC	(200)	3.96	0.028308	0.025286	69.0
20 min CNCs-MCC	(200)	4.02	0.035053	0.038726	73.2
30 min CNCs-MCC	(200)	3.90	0.031703	0.032078	73.0

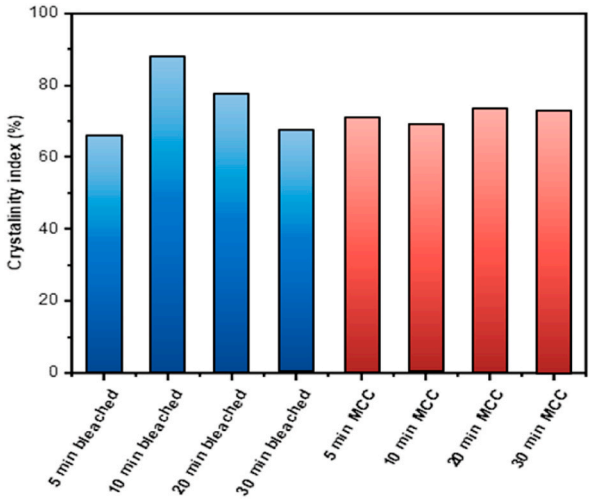

Fig. 3. Crystallinity index of CNCs-NRFs and CNCs-MCC samples.

Table 2
Degree of crystallinity of extracted CNCs based on treatment method and its comparison with different lignocellulosic sources.

Cellulose sources	Treatment method	Degree of crystallinity (%)	Refs
Eichhornia crassipes	Acidic hydrolysis (10 min)	87.60	This work
Water hyacinth	Chemical/mechanical processes	76.70	[38]
Soy hulls	Acidic hydrolysis (30 min)	73.50	[39]
Water Hyacinth	Chemical treatments	78.80	[40]
Sugarcane bagasse	Acidic hydrolysis (30 min)	87.50	[41]
Eucalyptus kraft pulp	Acidic hydrolysis	82.08	[42]
Eucalyptus kraft pulp	Chemical treatments	80.00	[43]
Eucalyptus kraft pulp	Chemical treatments	N/A	[44]
Eucalyptus kraft pulp	Acidic hydrolysis	N/A	[45]
Eucalyptus kraft pulp	Acidic hydrolysis	80.60	[46]

peaks of –OH (stretching and bending) and C–*O*–C for reduced [34,49,50]. Meanwhile, another prominent feature in the absorption peak at 727 cm^{-1} which disappeared under the acid treatment time, evidencing that most of hemicelluloses and aromatic skeletal for lignin were removed significantly [36]. However, it was noticed from Fig. 4(a) that there was no change in the FT-IR spectrum for pulped fiber when compared to the spectrum of native fiber [51]. Fig. 4(b–c) showed the effect of acid hydrolysis duration ranging from 5 to 30 min on the functional groups of CNCs extracted from NRFs and MCC. The reduction in the intensity of absorption peaks of –OH stretching (3436 cm^{-1}), –OH bending (~1640 cm^{-1}) and C–*O*–C stretching (1057 cm^{-1}) [52,53] when increasing the duration of acid hydrolysis illustrates the increase in the amount of CNCs extracted from both cellulose sources.

3.3. TEM analysis

TEM images can provide additional insight into the effect of acid hydrolysis duration on the structure and the size of CNCs extracted from NRFs and MCC, as shown in Fig. 5. The length and diameter of CNCs for both cellulose sources were listed in Table 3 and estimated by the Image J program $\left(\text{Aspect ratio} = \frac{\text{length of rods,L}}{\text{Diameter of rods,d}}\right)$ [54]. For better visualization, each photograph was shown at two

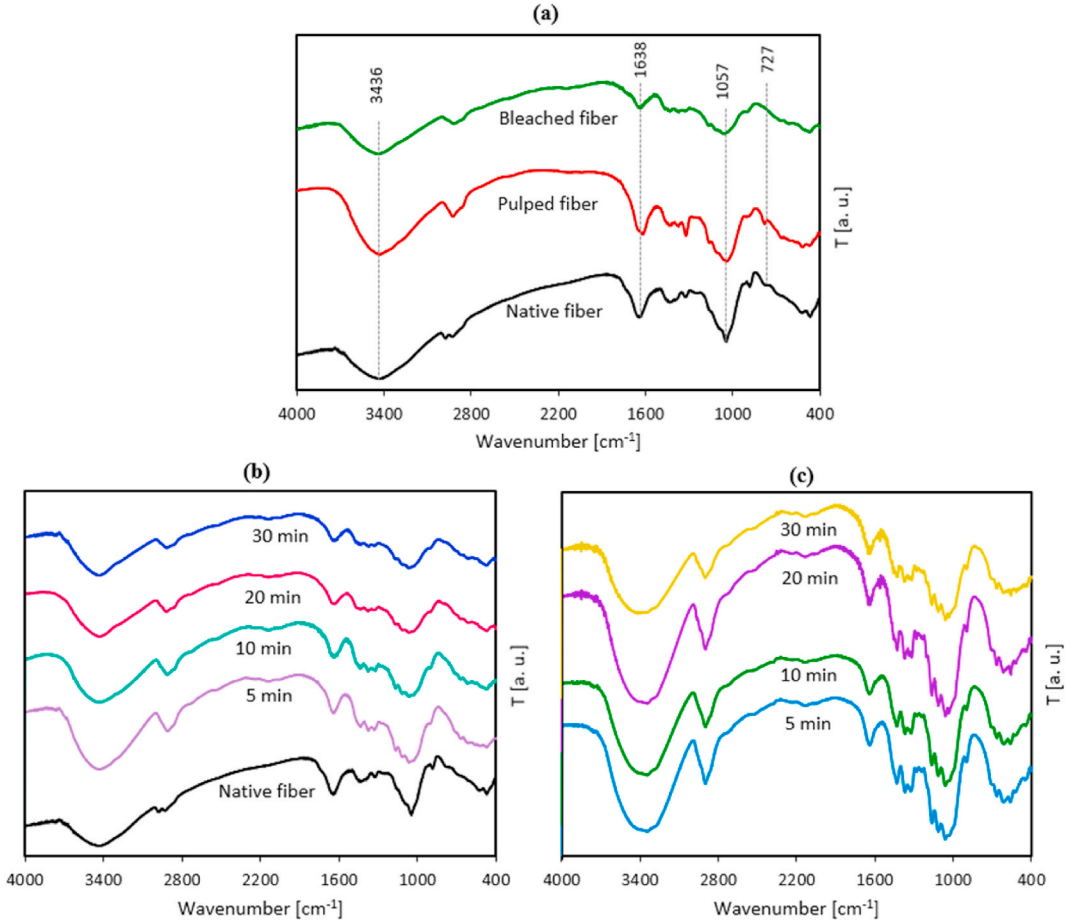

Fig. 4. FTIR spectra for (a) native, pulped and bleached NRFs, (b) CNCs-based NRFs, and (c) CNCs-based MCC.

magnifications. As can be seen in Fig. 5(a and b), the high magnification images showed that acid hydrolysis of CNCs-NRFs or CNCs-MCC at 5 min yielded fibril-like clusters in the case of CNCs extracted from NRFs with an average length of about 231 nm and width of 29 nm, indicating that the fibrous structure was achieved. The CNCs extracted from MCC produced meshed rods-like structure morphology with an average length of about 205 nm and a width of 24. These outcomes agree with the findings reported elsewhere [55]. By increasing the acid hydrolysis duration up to 20 min, the average size of extracted CNCs reduced to ~108 nm in length and 20 nm in width for NRFs and ~122 nm in length and 12 nm in width for CNCs-MCC, as depicted in Fig. 5(a and b) and Table 3. This indicated that increasing the processing time or duration of acid hydrolysis has a significant impact on the yield and the structure of CNCs in the magnified images. Interestingly, the average size of CNCs, whether extracted from NRFs or MCC, was smaller and one-dimensional when the acid hydrolysis duration increased to 30 min (Table 3). This indicated that a spherical morphology was probably formed for both types of CNCs, providing evidence that acid hydrolysis time has a positive impact on CNCs morphology. This result is consistent with that obtained by XRD patterns. On the other hand, Wulandari et al. [29] reported that the crystalline part of nanocellulose could be damaged during the acid hydrolysis process, and therefore the crystallinity index decreased. General speaking, it can be concluded that the size distribution of extracted CNCs was more affected by increasing the duration of acid hydrolysis and the optimum time was 20 min.

3.4. Zeta potential analysis

The zeta potential was utilized to determine the strength of attractive or repulsion between CNCs nanoparticles which was considered to be an essential parameter of the characterization of the materials stability in colloidal system [56]. It can be seen from Fig. 6 that the zeta potential values obtained under all conditions were negative. Moreover, it was found that their values were decreased with increasing the acidic hydrolysis durations from −32.9 mV to - 41 mV for CNCs-NRFs and from −27.8 mV to −35.5 mV for CNCs-MCC at 5 and 30 min, respectively. This implies that the higher zeta potential values at lower acidic hydrolysis time, strong electrostatic repulsion can prevent CNCs particles from getting close, therefore increasing their stability in colloidal system [56]. However, the stability of CNCs particles was affected by the increasing of acid hydrolysis treatment times.

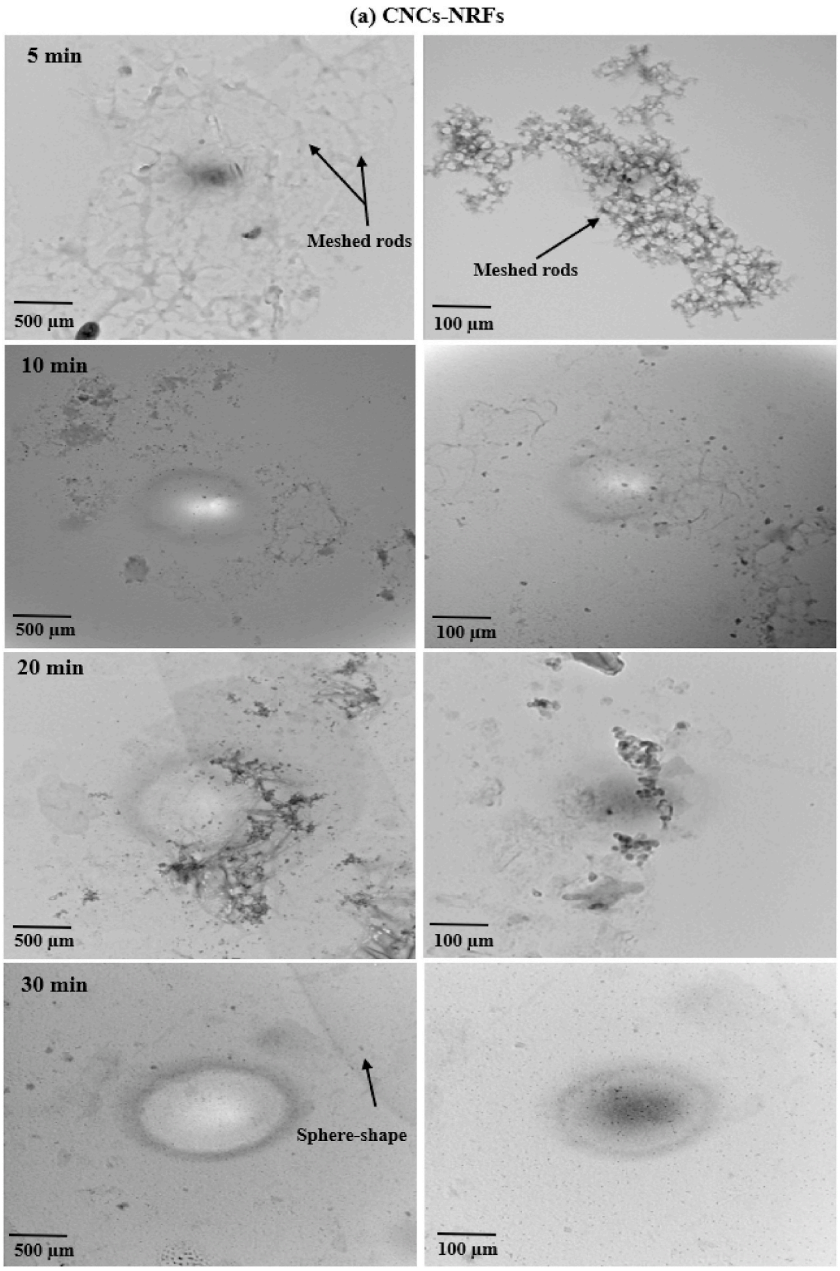

Fig. 5. TEM images of CNCs extracted from NRFs (a) and MCC (b) by acid hydrolysis with variable durations ranging from 5 to 30 min.

3.5. XPS analysis

Table 4 showed the results of elemental analysis for 5 min and 30 min acid hydrolysis for CNCs-NRFs and CNCs-MCC samples. It was found that the 5 min and 30 min acid hydrolysis for CNCs-NRFs, as well as 5 min for CNCs-MCC results in samples containing approximately 40 at% oxygen and 60 at% carbon. The 30 min acid hydrolysis for CNCs-MCC results in 35 at% and 64% oxygen and carbon, respectively. However, the 30 min acid hydrolysis for both CNCs investigated demonstrated only negligible background traces of nitrogen content. The XPS curves of Fig. 7 showed two sharp peaks located at binding energies of about 286.08 eV and 533.08 eV corresponding to C 1s and O 1s, respectively [57]. Furthermore, it was noticed that the C 1s and O 1s intensities for CNCs-NRFs and CNCs-MCC increased with the duration of acid hydrolysis, indicating that the morphology of CNCs may be affected. This outcome agrees with that obtained by XRD and TEM observations. The high-resolution (deconvoluted) spectra of C 1s and O 1s were represented in Fig. 8(a–h). The deconvoluted C1s XPS spectra of pure cellulose exhibited only two peaks related to the C–O of alcohol and ether

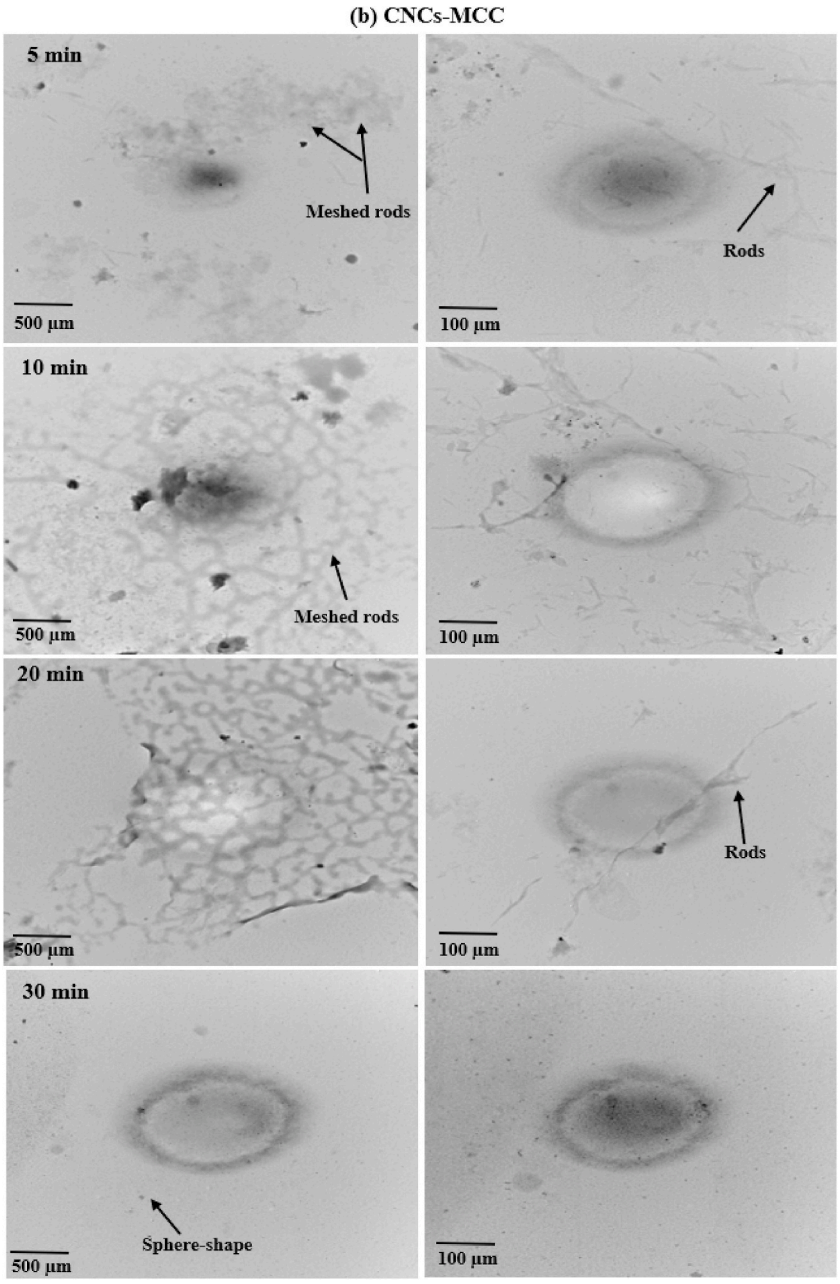

Fig. 5. (*continued*).

Table 3
Average size and aspect ratios of CNCs-NRFs and CNCs-MCC obtained from TEM observations.

Fiber type		Acidic hydrolysis duration (min)			
		5	10	20	30
Average size for CNCs-NRFs, nm	Length	230.70	181.91	107.84	9.65
	Width	28.94	24.15	19.83	
	Aspect ratio	7.97	7.53	5.43	–
Average size for CNCs-MCC, nm	Length	204.85	155.35	121.90	8.04
	Width	24.20	14.93	11.90	
	Aspect ratio	8.46	10.40	10.24	–

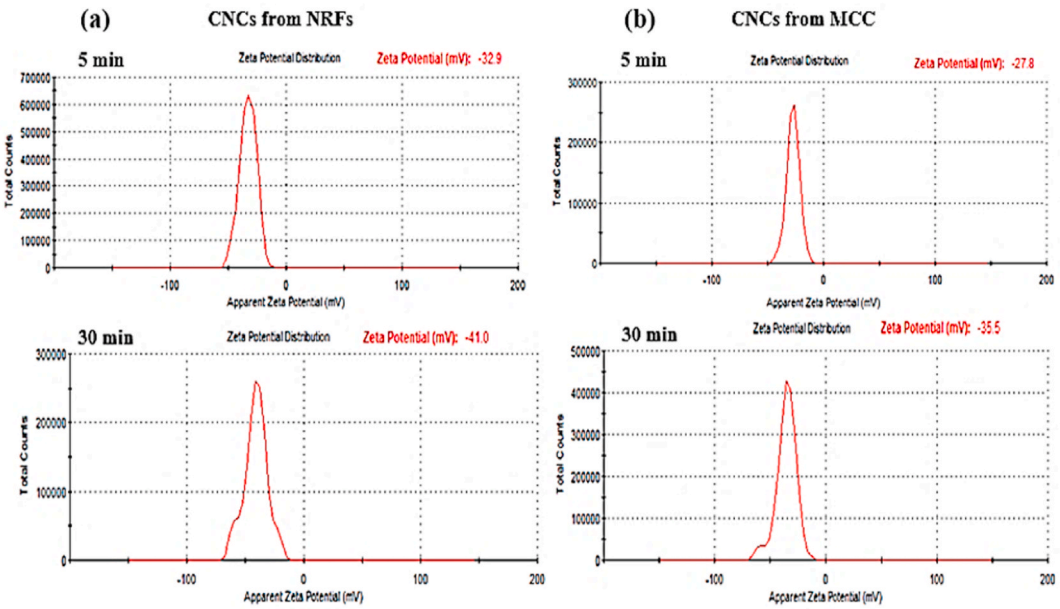

Fig. 6. Zeta potential analysis for CNCs-NRFs (a) and CNCs-MCC (b) at 5 and 30 min acidic hydrolysis.

Table 4
XPS related parameters for CNCs extracted from NRFs and MCC.

Specimen name	*Element*	*Peak B.E, eV*	*FWHM, eV*	*Area, eV*	*Atomic, %*
5 min *(NRFs)*	O 1s	533.37	3.55	258200.9	41.96
	C 1s	286.93	4.20	139917.2	58.04
30 min *(NRFs)*	O 1s	532.99	3.28	380430.2	38.84
	C 1s	286.16	4.27	232274.3	60.52
5 min MCC	O 1s	533.25	3.18	305468.4	40.18
	C 1s	286.88	3.72	178168.2	59.82
30 min MCC	O 1s	533.1	3.21	368235.2	35.17
	C 1s	286.29	4.04	261298.3	63.69

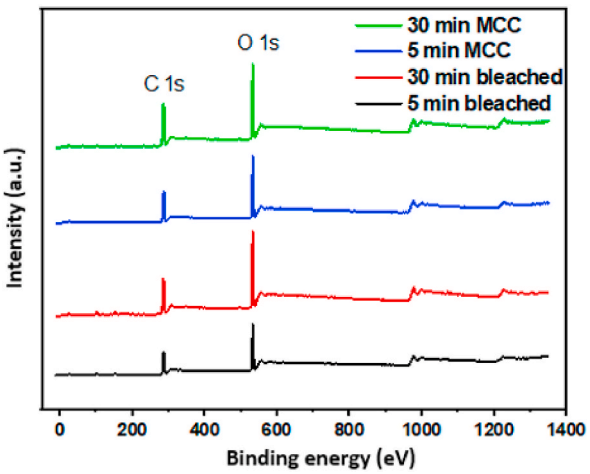

Fig. 7. XPS survey scan for CNCs extracted from NRFs and MCC.

groups and O–C–O for acetal moieties. The XPS analysis of the CNCs-NRFs and CNCs-MCC showed three peaks at ~284, 286, and 287 eV. These peaks were attributed to the C1 carbon bonded to other carbon or hydrogen atom (C–C or C–H), C2 carbon bonded to oxygen atom (C–O) and C3 carbons attached to two oxygen atoms or a carbonyl group (C═O and/or O–C═O). The C1 peak was mainly

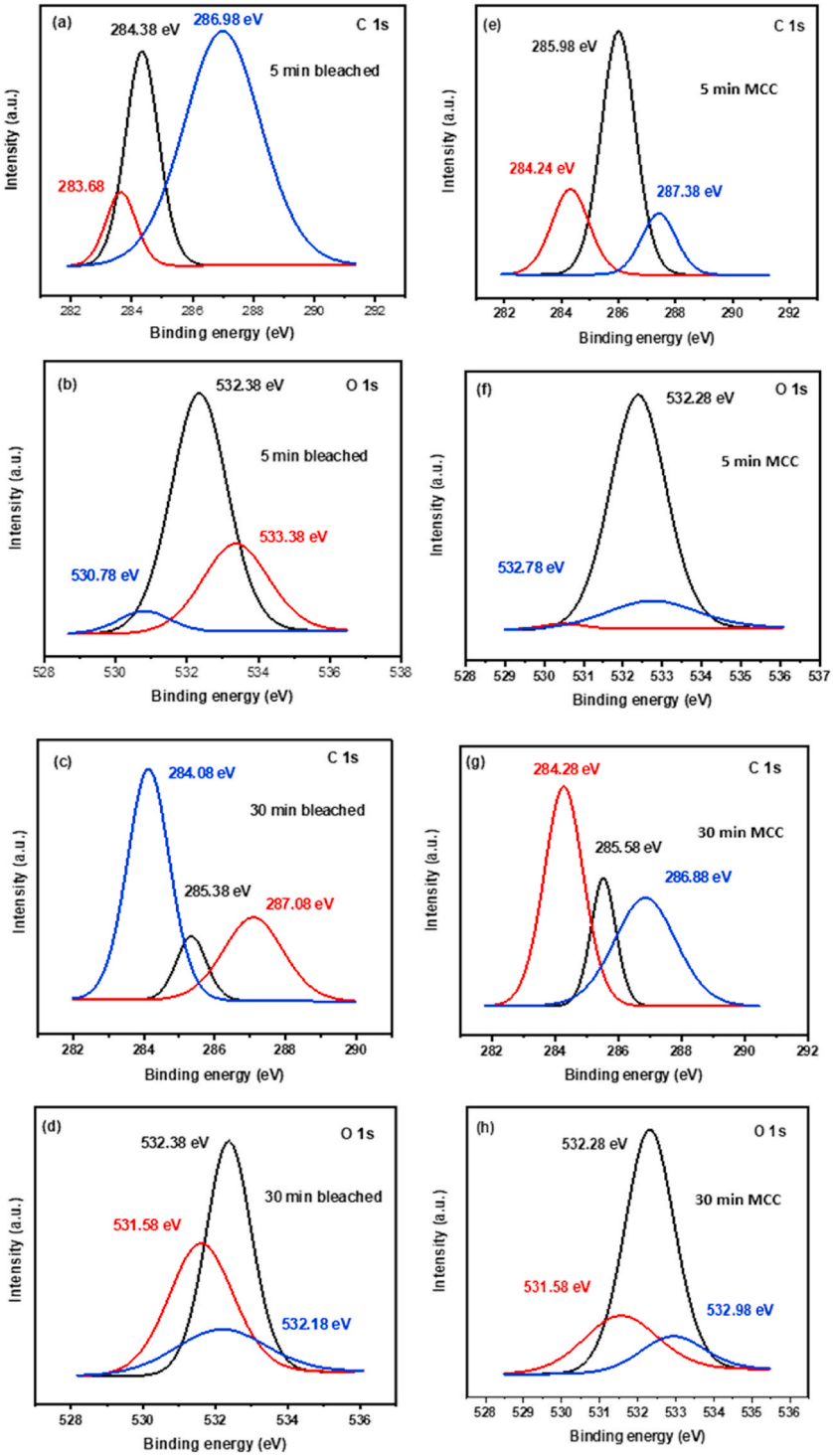

Fig. 8. Deconvoluted spectra for a) C 1s of 5 min CNCs-NRFs b) O 1s of 5 min CNCs-NRFs, c) C 1s of 30 min CNCs-NRFs d) O 1s of 30 min CNCs-NRFs, e) C 1s of 5 min CNCs-MCC, f) O 1s of 5 min CNCs-MCC, g) C 1s of 30 min CNCs-MCC, h) O 1s of 30 min CNCs-MCC.

ascribed to cellulose [58–60]. The amount of extracted cellulose can be quantified from the area under C1 curve. The binding energy (BE) values, peak area, intensity, and FWHM for all samples were presented in Table 5. It was observed from Table 5, the area under C1 curve increased as the acidic hydrolysis duration of CNCs-NRFs increased, thereby leading to increase the amount of extracted cellulose. The C1 area of both CNCs-NRFs and CNCs-MCC was approximately the same. This confirmed that the acid hydrolysis duration

Table 5
The BE values, peak area, intensity, and FWHM for all samples.

Specimen name	*Carbon type*	*Peak B E, eV*	*Intensity CPS*	*Area*	*FWHM*
5 min *(NRFs)*	C1	283.63	571	724	1.18
	C2	284.38	1664	2335	1.29
	C3	286.98	1820	5881	2.98
30 min *(NRFs)*	C1	284.08	6726	10330	1.4
	C2	285.38	1889	2117	1.01
	C3	287.08	2419	5236	1.98
5 min MCC	C1	284.24	2649	4438	1.54
	C2	285.98	7523	11527	1.42
	C3	287.38	1893	2925	1.42
30 min MCC	C1	284.28	6844	10788	1.46
	C2	285.58	3980	4002	0.93
	C3	286.88	3366	8334	2.29

(i.e. 30 min) was sufficient to extract the cellulose. Referring to the amount of the C2 (C–O), it was observed that the amount the C2 remained approximately constant. This can be explained as follows, by increasing the acid hydrolysis duration, the amount of extracted cellulose increased. However, when CNCs-MCC sample was subjected to prolonged acid hydrolysis duration, more carbon atoms were bonded to oxygen atom. For the C3 (C═O and/or O–C═O), the same behavior as C2 was observed. For CNCs-NRFs samples, it was observed that the C–O signals increase with the acid hydrolysis duration, as depicted in Fig. 6(a–d) [61,62]. The same behavior was noticed for CNCs-MCC samples (Fig. 8(e–h)). Consequently, it can be concluded that the predominant components of extracted CNCs were carbon and oxygen.

4. Conclusions

In this manuscript, renewable cellulose nanocrystals (CNCs) were successfully extracted from Nile roses fibers (*Eichhornia crassipes*) considered as agricultural residue recycling by acid hydrolysis approach to be used in a variety of potential applications. Nile roses fibers (NRFs) were initially subjected to alkaline pulping and bleaching pretreatments, followed by acid hydrolysis ranging between 5 &30 min. Microcrystalline cellulose (MCC) was used as control. The crystallinity index and morphology of CNCs extracted from NRFs were characterized by various techniques; namely: XRD, FT-IR, TEM, and XPS analysis. The data obtained from XRD indicated that the highest crystallinity index was observed at acid hydrolysis duration of 10 min, and then started to reduce. FT-IR spectra illustrated that the intensities of the basic absorption peaks of bleached samples reduced with increasing acid hydrolysis time, proving that most of the hemicellulose and aromatic skeletal for lignin were removed. Also, TEM visualizations confirmed the fibril structure of CNCs with different sizes, depending on the acid hydrolysis duration. However, a spherical morphology of the CMCs-derived CNCs was formed behind 20 min. XPS outcomes showed that the main constituents of extracted CNCs are carbon and oxygen. This work depicts a new employment for CNCs extracted from agro-residues in promising applications such as bio-membranes for water remediation, food packaging, and hydrogels for biomedical purposes.

Author contribution statement

Mohamed H. Hemida, M.M. Ibrahim, Sherif Mehanny, Eid N. Abd EL Rahman: Conceived and designed the experiments; Performed the experiments; Analyzed and interpreted the data; Contributed reagents, materials, analysis tools or data.

Hesham Moustafa, Alain Dufresne: Analyzed and interpreted the data; Wrote the paper.

Mohamed Morsy: Contributed reagents, materials, analysis tools or data; Wrote the paper.

Data availability statement

The authors are unable or have chosen not to specify which data has been used.

Additional information

No additional information is available for this paper.

Declaration of competing interest

The authors have no conflict of interest to declare in this study.

Acknowledgements

The authors would like to thank Cairo University -Egypt, for the financial support underlying PhD thesis of Mohamed H. Hemida.

References

[1] A.M. Negm, N. Shareef, Waste Management in MENA Regions, 2019.
[2] M.E. Alves Fidelis, T.V.C. Pereira, O.D.F.M. Gomes, F. De Andrade Silva, R.D. Toledo Filho, The effect of fiber morphology on the tensile strength of natural fibers, J. Mater. Res. Technol. 2 (2013) 149–157, https://doi.org/10.1016/j.jmrt.2013.02.003.
[3] Z. Anwar, M. Gulfraz, M. Irshad, Agro-industrial lignocellulosic biomass a key to unlock the future bio-energy: a brief review, J. Radiat. Res. Appl. Sci. 7 (2014) 163–173, https://doi.org/10.1016/j.jrras.2014.02.003.
[4] J. Huang, S. Qiu, D. Rodrigue, Parameters estimation and fatigue life prediction of sisal fibre reinforced foam concrete, J. Mater. Res. Technol. 20 (2022) 381–396, https://doi.org/10.1016/j.jmrt.2022.07.096.
[5] J. Wang, J. Fu, W. Song, Y. Zhang, Effect of rice husk ash (RHA) dosage on pore structural and mechanical properties of cemented paste backfill, J. Mater. Res. Technol. 17 (2022) 840–851, https://doi.org/10.1016/j.jmrt.2022.01.044.
[6] C.M. Ajila, S.K. Brar, M. Verma, R.D. Tyagi, S. Godbout, J.R. Valéro, Bio-processing of agro-byproducts to animal feed, Crit. Rev. Biotechnol. 32 (2012) 382–400, https://doi.org/10.3109/07388551.2012.659172.
[7] M.H. El-Moayed, J. Kühn, S.H. Lee, M. Farag, S. Mehanny, Potential of Lignin Valorization with Emphasis on Bioepoxy Production. Book: Lignin - Chemistry, Structure, and Application, Dec 2022, https://doi.org/10.5772/intechopen.108263.
[8] M.I. Voronova, O.V. Surov, A.V. Afineevskii, A.G. Zakharov, Properties of polyacrylamide composites reinforced by cellulose nanocrystals, Heliyon 6 (2020), https://doi.org/10.1016/j.heliyon.2020.e05529.
[9] H. Moustafa, C. Guizani, A. Dufresne, Sustainable biodegradable coffee grounds filler and its effect on the hydrophobicity, mechanical and thermal properties of biodegradable PBAT composites, J. Appl. Polym. Sci. 134 (2017), https://doi.org/10.1002/app.44498.
[10] A.E.A.A. El-Wakil, H. Moustafa, A.M. Youssef, Antimicrobial low-density polyethylene/low-density polyethylene-grafted acrylic acid biocomposites based on rice bran with tea tree oil for food packaging applications, J. Thermoplast. Compos. Mater. (2020), https://doi.org/10.1177/0892705720925140.
[11] H. Moustafa, A.E.-A.A. El-Wakil, M.T. Nour, A.M. Youssef, Kenaf fibre treatment and its impact on the static, dynamic, hydrophobicity and barrier properties of sustainable polystyrene biocomposites, RSC Adv. 10 (2020) 29296–29305, https://doi.org/10.1039/D0RA05334A.
[12] H. Elsayed, M. Farag, H. Megahed, S. Mehanny, Influence of flax fibers on properties of starch-based composites, ASME (2012). https://doi.org/10.1115/IMECE2012-89628.
[13] Z Ammar, H Ibrahim, M Adly, I Sarris, S Mehanny, Influence of Natural Fiber Content on the Frictional Material of Brake Pads—A Review, Journal of Composites Science 7 (2) (2023) 72. https://doi.org/10.3390/jcs702007.
[14] A.O. Sulyman, A. Igunnu, S.O. Malomo, Isolation, purification and characterization of cellulase produced by Aspergillus Niger cultured on Arachis hypogaea shells, Heliyon 6 (2020), e05668, https://doi.org/10.1016/j.heliyon.2020.e05668.
[15] M. Hannon, J. Gimpel, M. Tran, B. Rasala, S. Mayfield, Biofuels from algae: challenges and potential, Biofuels 1 (2010) 763–784, https://doi.org/10.4155/bfs.10.44.
[16] W.T. Tsai, S.C. Liu, C.H. Hsieh, Preparation and fuel properties of biochars from the pyrolysis of exhausted coffee residue, J. Anal. Appl. Pyrolysis 93 (2012) 63–67, https://doi.org/10.1016/j.jaap.2011.09.010.
[17] H. Moustafa, E.M. Ahmed, M. Morsy, Bio-based antibacterial packaging from decorated bagasse papers with natural rosin and synthesised GO-Ag nanoparticles, Mater. Technol. 37 (2022) 2766–2776, https://doi.org/10.1080/10667857.2022.2074939.
[18] A.A. Alfi, N.A. Alamrani, O.A. Azher, R.M. Snari, H.M. Abumelha, Z.A. Al-Ahmed, N.M. El-Metwaly, Development of carbon dots sensor dipstick from sugarcane bagasse agricultural waste toward all-cellulose-derived tetracycline sensor, J. Mater. Res. Technol. 19 (2022) 4697–4707, https://doi.org/10.1016/j.jmrt.2022.06.150.
[19] R. Zuluaga, J.L. Putaux, J. Cruz, J. Vélez, I. Mondragon, P. Gañán, Cellulose microfibrils from banana rachis: effect of alkaline treatments on structural and morphological features, Carbohydr. Polym. 76 (2009) 51–59, https://doi.org/10.1016/j.carbpol.2008.09.024.
[20] M.H. Hamidon, M.T.H. Sultan, A.H. Ariffin, A.U.M. Shah, Effects of fibre treatment on mechanical properties of kenaf fibre reinforced composites: a review, J. Mater. Res. Technol. 8 (2019) 3327–3337, https://doi.org/10.1016/j.jmrt.2019.04.012.
[21] L.U.S. Faria, B.J.S. Pacheco, G.C. Oliveira, J.L. Silva, Production of cellulose nanocrystals from pineapple crown fibers through alkaline pretreatment and acid hydrolysis under different conditions, J. Mater. Res. Technol. 9 (2020) 12346–12353, https://doi.org/10.1016/j.jmrt.2020.08.093.
[22] F. Hemmati, S.M. Jafari, M. Kashaninejad, M. Barani Motlagh, Synthesis and characterization of cellulose nanocrystals derived from walnut shell agricultural residues, Int. J. Biol. Macromol. 120 (2018) 1216–1224, https://doi.org/10.1016/j.ijbiomac.2018.09.012.
[23] H. Moustafa, N.A. Darwish, M.A. Nour, A.M. Youssef, Biodegradable date stones filler for enhancing mechanical, dynamic, and flame retardant properties of polyamide-6 biocomposites, Polym. Compos. 39 (2018) 1978–1987, https://doi.org/10.1002/pc.24157.
[24] D. Klemm, B. Heublein, H.P. Fink, A. Bohn, Cellulose: fascinating biopolymer and sustainable raw material, Angew. Chem. Int. Ed. 44 (2005) 3358–3393, https://doi.org/10.1002/anie.200460587.
[25] E.M. Eid, K.H. Shaltout, Population dynamics of Eichhornia crassipes (C. Mart.) Solms in the nile Delta, Egypt, Plant Species Biol. 32 (2017) 279–291, https://doi.org/10.1111/1442-1984.12154.
[26] A.G. Bayrakci, G. Koçar, Second-generation bioethanol production from water hyacinth and duckweed in Izmir: a case study, Renew. Sustain. Energy Rev. 30 (2014) 306–316, https://doi.org/10.1016/j.rser.2013.10.011.
[27] B.L. Peng, N. Dhar, H.L. Liu, K.C. Tam, Chemistry and applications of nanocrystalline cellulose and its derivatives: a nanotechnology perspective, Can. J. Chem. Eng. 89 (2011) 1191–1206, https://doi.org/10.1002/cjce.20554.
[28] N.L. Garcia de Rodriguez, W. Thielemans, A. Dufresne, Sisal cellulose whiskers reinforced polyvinyl acetate nanocomposites, Cellulose 13 (2006) 261–270, https://doi.org/10.1007/s10570-005-9039-7.
[29] W.T. Wulandari, A. Rochliadi, I.M. Arcana, Nanocellulose prepared by acid hydrolysis of isolated cellulose from sugarcane bagasse, IOP Conf. Ser. Mater. Sci. Eng. 107 (2016), https://doi.org/10.1088/1757-899X/107/1/012045.
[30] M.A. Mahmud, F.R. Anannya, Sugarcane bagasse - a source of cellulosic fiber for diverse applications, Heliyon 7 (2021), e07771, https://doi.org/10.1016/j.heliyon.2021.e07771.
[31] Kusmono, R.F. Listyanda, M.W. Wildan, M.N. Ilman, Preparation and characterization of cellulose nanocrystal extracted from ramie fibers by sulfuric acid hydrolysis, Heliyon 6 (2020), e05486, https://doi.org/10.1016/j.heliyon.2020.e05486.
[32] E. de M. Teixeira, T.J. Bondancia, K.B.R. Teodoro, A.C. Corrêa, J.M. Marconcini, L.H.C. Mattoso, Sugarcane bagasse whiskers: extraction and characterizations, Ind. Crop. Prod. 33 (2011) 63–66, https://doi.org/10.1016/j.indcrop.2010.08.009.
[33] W.H. Wan Ishak, N.A. Rosli, I. Ahmad, S. Ramli, M.C.I. Mohd Amin, Drug delivery and in vitro biocompatibility studies of gelatin-nanocellulose smart hydrogels cross-linked with gamma radiation, J. Mater. Res. Technol. 15 (2021) 7145–7157, https://doi.org/10.1016/j.jmrt.2021.11.095.
[34] H. Moustafa, H. Isawi, S.M.A. El, Environmental Nanotechnology , Monitoring & Management Utilization of PVA nano-membrane based synthesized magnetic GO-Ni-Fe 2 O 4 nanoparticles for removal of heavy metals from water resources, Environ. Nanotechnol. Monit. Manag. 18 (2022), 100696, https://doi.org/10.1016/j.enmm.2022.100696.
[35] A. Adel, A. El-Shafei, A. Ibrahim, M. Al-Shemy, Extraction of oxidized nanocellulose from date palm (Phoenix Dactylifera L.) sheath fibers: influence of CI and CII polymorphs on the properties of chitosan/bionanocomposite films, Ind. Crop. Prod. 124 (2018) 155–165, https://doi.org/10.1016/j.indcrop.2018.07.073.
[36] S. Mehanny, E.E. Abu-El Magd, M. Ibrahim, M. Farag, R. Gil-San-Millan, J. Navarro, A.E.H. El Habbak, E. El-Kashif, Extraction and characterization of nanocellulose from three types of palm residues, J. Mater. Res. Technol. 10 (2021) 526–537, https://doi.org/10.1016/j.jmrt.2020.12.027.
[37] M. Morsy, A. Elzwawy, A.I. Abdel-salam, M.M. Mokhtar, A.B. El Basaty, Diamond & Related Materials the humidity sensing characteristics of PANI-titania nanotube-rGO ternary nanocomposite, Diam. Relat. Mater. 126 (2022), 109040, https://doi.org/10.1016/j.diamond.2022.109040.
[38] S. Tanpichai, S. Mekcham, C. Kongwittaya, W. Kiwijaroun, K. Thongdonsun, C. Thongdeelerd, A. Boonmahitthisud, Extraction of nanofibrillated cellulose from water hyacinth using a high speed homogenizer, J. Nat. Fibers 19 (2022) 5676–5696, https://doi.org/10.1080/15440478.2021.1889432.

[39] W.P. Flauzino Neto, H.A. Silvério, N.O. Dantas, D. Pasquini, Extraction and characterization of cellulose nanocrystals from agro-industrial residue - Soy hulls, Ind. Crop. Prod. 42 (2013) 480–488, https://doi.org/10.1016/j.indcrop.2012.06.041.
[40] S. Tanpichai, S.K. Biswas, S. Witayakran, H. Yano, Water hyacinth: a sustainable lignin-poor cellulose source for the production of cellulose nanofibers, ACS Sustain. Chem. Eng. 7 (2019) 18884–18893, https://doi.org/10.1021/acssuschemeng.9b04095.
[41] E. de M. Teixeira, T.J. Bondancia, K.B.R. Teodoro, A.C. Corrêa, J.M. Marconcini, L.H.C. Mattoso, Sugarcane bagasse whiskers: extraction and characterizations, Ind. Crop. Prod. 33 (2011) 63–66, https://doi.org/10.1016/j.indcrop.2010.08.009.
[42] H. Wang, H. Du, K. Liu, H. Liu, T. Xu, S. Zhang, X. Chen, R. Zhang, H. Li, H. Xie, X. Zhang, C. Si, Sustainable preparation of bifunctional cellulose nanocrystals via mixed H2SO4/formic acid hydrolysis, Carbohydr. Polym. 266 (2021), https://doi.org/10.1016/j.carbpol.2021.118107.
[43] W. Liu, H. Du, H. Liu, H. Xie, T. Xu, X. Zhao, Y. Liu, X. Zhang, C. Si, Highly efficient and sustainable preparation of carboxylic and thermostable cellulose nanocrystals via FeCl3-catalyzed innocuous citric acid hydrolysis, ACS Sustain. Chem. Eng. 8 (2020) 16691–16700, https://doi.org/10.1021/acssuschemeng.0c06561.
[44] X. Yang, H. Xie, H. Du, X. Zhang, Z. Zou, Y. Zou, W. Liu, H. Lan, X. Zhang, C. Si, Facile extraction of thermally stable and dispersible cellulose nanocrystals with high yield via a green and recyclable FeCl3-catalyzed Deep eutectic Solvent system, ACS Sustain. Chem. Eng. 7 (2019) 7200–7208, https://doi.org/10.1021/acssuschemeng.9b00209.
[45] H. Wang, H. Xie, H. Du, X. Wang, W. Liu, Y. Duan, X. Zhang, L. Sun, X. Zhang, C. Si, Highly efficient preparation of functional and thermostable cellulose nanocrystals via H2SO4 intensified acetic acid hydrolysis, Carbohydr. Polym. 239 (2020), 116233, https://doi.org/10.1016/j.carbpol.2020.116233.
[46] H. Xie, Z. Zou, H. Du, X. Zhang, X. Wang, X. Yang, H. Wang, G. Li, L. Li, C. Si, Preparation of thermally stable and surface-functionalized cellulose nanocrystals via mixed H2SO4/Oxalic acid hydrolysis, Carbohydr. Polym. 223 (2019), 115116, https://doi.org/10.1016/j.carbpol.2019.115116.
[47] M.M. Ibrahim, H. Moustafa, E.N.A. El Rahman, S. Mehanny, M.H. Hemida, E. El-Kashif, Reinforcement of starch based biodegradable composite using Nile rose residues, J. Mater. Res. Technol. 9 (2020) 6160–6171, https://doi.org/10.1016/j.jmrt.2020.04.018.
[48] M.A.N. Moustafa Hesham, Ahmed M. Youssef, Investigation of morphology, mechanical, thermal and flame retardant properties of an EVA/EPDM blend by combination of organoclay with Na+- tripolyphosphate, RSC Adv. 6 (2016), 36467, https://doi.org/10.1039/c6ra03341e.
[49] Hesham Moustafa, Nabila A. Darwish, Ahmed M. Youssef, Sameh M. Reda, Abd El-Aziz A. El-Wakil1, High-performance of nanoparticles and their effects on the, Egypt, J. Chem. 21 (2018) 23–32.
[50] H. Du, W. Liu, M. Zhang, C. Si, X. Zhang, B. Li, Cellulose nanocrystals and cellulose nanofibrils based hydrogels for biomedical applications, Carbohydr. Polym. 209 (2019) 130–144, https://doi.org/10.1016/j.carbpol.2019.01.020.
[51] H. Moustafa, N.A. Darwish, A.M. Youssef, Rational formulations of sustainable polyurethane/chitin/rosin composites reinforced with ZnO-doped-SiO2 nanoparticles for green packaging applications, Food Chem. 371 (2022), 131193, https://doi.org/10.1016/j.foodchem.2021.131193.
[52] H. Moustafa, A.M. Karmalawi, A.M. Youssef, Development of dapsone-capped TiO2 hybrid nanocomposites and their effects on the UV radiation, mechanical, thermal properties and antibacterial activity of PVA bionanocomposites, Environ. Nanotechnol. Monit. Manag. 16 (2021), 100482, https://doi.org/10.1016/j.enmm.2021.100482.
[53] H. Moustafa, S. Duquesne, B. Haidar, M.F.F. Vallat, Influence of the degree of exfoliation of an organoclay on the flame-retardant properties of cross-linked ethylene-co-Propylene-co-diene monomer-g-Maleic anhydride-based composites, Polym. Compos. 38 (2017) 966–973, https://doi.org/10.1002/pc.23659.
[54] I. Strength, Estimation of Aspect Ratio of Cellulose Nanocrystals by Viscosity Measurement : Influence of Aspect Ratio, (n.d.).
[55] S. Mehanny, E.E. Abu-El Magd, S. Sorbara, J. Navarro, R. Gil-San-millan, Spanish poplar biomass as a precursor for nanocellulose extraction, Appl. Sci. 11 (2021), https://doi.org/10.3390/app11156863.
[56] X. Yu, Y. Jiang, Q. Wu, Z. Wei, X. Lin, Y. Chen, Preparation and characterization of cellulose nanocrystal extraction from pennisetum hydridum fertilized by municipal Sewage Sludge via sulfuric acid hydrolysis, Front. Energy Res. 9 (2021) 1–10, https://doi.org/10.3389/fenrg.2021.774783.
[57] J.H. Jordan, M.W. Easson, B. Dien, S. Thompson, B.D. Condon, Extraction and characterization of nanocellulose crystals from cotton gin motes and cotton gin waste, Cellulose 26 (2019) 5959–5979, https://doi.org/10.1007/s10570-019-02533-7.
[58] B. Ly, W. Thielemans, A. Dufresne, D. Chaussy, M.N. Belgacem, Surface functionalization of cellulose fibres and their incorporation in renewable polymeric matrices Surface functionalization of cellulose fibres and their incorporation in renewable polymeric matrices, Compos. Sci. Technol. 68 (2008) 3193–3201, https://doi.org/10.1016/j.compscitech.2008.07.018.
[59] J.C. Bastidas, R. Venditti, J. Pawlak, R. Gilbert, Chemical Force Microscopy of Cellulosic Fibers, 2005, https://doi.org/10.1016/j.carbpol.2005.08.058.
[60] M. Azadfar, Surface Characterization of Powdered Cellulose Activated by Potassium Hydroxide in Dry Condition through Ball Milling, 2020, pp. 80–89.
[61] M. Smith, L. Scudiero, J. Espinal, J.S. McEwen, M. Garcia-Perez, Improving the Deconvolution and Interpretation of XPS Spectra from Chars by Ab Initio Calculations, Elsevier Ltd, 2016, https://doi.org/10.1016/j.carbon.2016.09.012.
[62] H. Idriss, On the wrong assignment of the XPS O1s signal at 531-532 eV attributed to oxygen vacancies in photo- and electro-catalysts for water splitting and other materials applications, Surf. Sci. 712 (2021), 121894, https://doi.org/10.1016/j.susc.2021.121894.